Multidecadally resolved polarity oscillations during a geomagnetic excursion

Yu-Min Chou[a,b,1,2], Xiuyang Jiang[c,1], Qingsong Liu[b,d,1], Hsun-Ming Hu[a], Chung-Che Wu[a], Jianxing Liu[d,e], Zhaoxia Jiang[f], Teh-Quei Lee[g], Chun-Chieh Wang[h], Yen-Fang Song[h], Cheng-Cheng Chiang[h], Liangcheng Tan[i,j], Mahjoor A. Lone[a], Yongxin Pan[k], Rixiang Zhu[k], Yaoqi He[l], Yu-Chen Chou[a], An-Hung Tan[m], Andrew P. Roberts[n], Xiang Zhao[n], and Chuan-Chou Shen[a,o,2]

[a]High-Precision Mass Spectrometry and Environment Change Laboratory, Department of Geosciences, National Taiwan University, 10617 Taipei, Taiwan, Republic of China; [b]Department of Ocean Science and Engineering, Southern University of Science and Technology, 518055 Shenzhen, People's Republic of China; [c]Key Laboratory of Humid Subtropical Eco-Geographical Processes, Ministry of Education, College of Geography Science, Fujian Normal University, 350117 Fuzhou, People's Republic of China; [d]Laboratory for Marine Geology, Qingdao National Oceanography Laboratory for Science and Technology, 266237 Qingdao, People's Republic of China; [e]Key Laboratory of Marine Sedimentology and Environmental Geology, First Institute of Oceanography, State Oceanic Administration, 266061 Qingdao, People's Republic of China; [f]College of Marine Geosciences, Ocean University of China, 266100 Qingdao, People's Republic of China; [g]Institute of Earth Sciences, Academia Sinica, 11529 Taipei, Taiwan, Republic of China; [h]National Synchrotron Radiation Research Center, 30076 Hsinchu, Taiwan, Republic of China; [i]State Key Laboratory of Loess and Quaternary Geology, Institute of Earth Environment, Chinese Academy of Sciences, 710061 Xi'an, People's Republic of China; [j]Institute of Global Environmental Change, Xi'an Jiaotong University, 710049 Xi'an, People's Republic of China; [k]Institute of Geology and Geophysics, Chinese Academy of Sciences, 100029 Beijing, People's Republic of China; [l]College of Tourism and Air Service, Guizhou Minzu University, 550025 Guiyang, People's Republic of China; [m]Department of Mechanical Engineering, Chien Hsin University of Science and Technology, 32097 Taoyuan, Taiwan, Republic of China; [n]Research School of Earth Sciences, Australian National University, Canberra, ACT 2601, Australia; and [o]Research Center for Future Earth, National Taiwan University, 10617 Taipei, Taiwan, Republic of China

Polarity reversals of the geomagnetic field have occurred through billions of years of Earth history and were first revealed in the early 20th century. Almost a century later, details of transitional field behavior during geomagnetic reversals and excursions remain poorly known. Here, we present a multidecadally resolved geomagnetic excursion record from a radioisotopically dated Chinese stalagmite at 107–91 thousand years before present with age precision of several decades. The duration of geomagnetic directional oscillations ranged from several centuries at 106–103 thousand years before present to millennia at 98–92 thousand years before present, with one abrupt reversal transition occurring in one to two centuries when the field was weakest. These features indicate prolonged geodynamo instability. Repeated asymmetrical interhemispheric polarity drifts associated with weak dipole fields likely originated in Earth's deep interior. If such rapid polarity changes occurred in future, they could severely affect satellites and human society.

multidecadally resolved polarity oscillations | geomagnetic excursion | abrupt reversal transition | asymmetrical interhemispheric polarity drifts | stalagmite U-Th dating

The geomagnetic field, which is generated by convection in Earth's liquid outer core (1), has existed for at least 3.45 billion y (2). It shields Earth from direct impact of solar wind and cosmic radiation, and its intensity and direction vary on timescales from milliseconds to tens of millions of years (3). Geomagnetic polarity reversals have occurred irregularly throughout Earth history (4), with the most recent polarity reversal defining the Matuyama–Brunhes boundary (MBB) that is astronomically dated at 773 ± 1 thousand years ago (ka) (5). At least 13 short-lived geomagnetic excursions have occurred since the MBB (e.g., the Laschamp excursion at 41 ka) (6).

Polarity reversals and excursions occur during periods with low geomagnetic field intensities (7, 8) (*SI Appendix*, Fig. S1), which could severely disorder the ionosphere, atmosphere, and biosphere (9, 10). Infrastructure and facilities for communication, transportation, and livelihoods can be threatened by such conditions (11). The contemporary geomagnetic field intensity is decreasing, and it has been suggested that a field reversal is impending (11, 12). Understanding details of transitional field behavior and obtaining precise estimates of transition duration are important for the Earth sciences, and they are also potentially significant for society and the biosphere.

Since the discovery of geomagnetic reversals in igneous rocks in the 1920s (13), diverse geological archives, such as lava flows, sedimentary rocks, and marine/lacustrine sediments, have been studied over recent decades (14, 15). Igneous rocks can provide ages of reversals and excursions via radioisotopic dating techniques (16, 17). However, intermittent eruption of igneous rocks hinders development of continuous records for studying transitional field configurations (18). Sedimentary records offer continuity (19) but are limited intrinsically by difficulties in obtaining radioisotopic chronologies and by smoothing of sedimentary paleomagnetic signals (20). Constraining details of transitional field structure during polarity reversals and excursions need accurate age control.

Speleothems have proven to be highly suitable for paleomagnetic reconstructions (21–23) because of their continuous

---

Significance

A stalagmite-based paleomagnetic record of the post-Blake excursion reveals details of repeated centennial–millennial interhemispheric polarity drifts and saw-tooth inclination oscillations during periods of low geomagnetic field intensity at 100 thousand years before present. One surprisingly abrupt centennial reversal transition occurred in 144 ± 58 years (2σ) and provides unprecedented evidence that raises fundamental questions about the speed of geomagnetic field shifts. Such rapid polarity changes could severely affect satellites and human society in the future if the current geomagnetic field intensity continues to decrease.

---

formation, short magnetization lock-in time, and minor post-depositional complications. Speleothem records have been obtained for the Laschamp excursion in North America (23) at 41.10 ± 0.35 ka and the Blake excursion (BE) in northern Spain (22) at 119–112 ka. Ongoing refinement of high-sensitivity superconducting magnetometry (24) and radioisotopic U-Th chronology (25, 26) offers the possibility of reconstructing geomagnetic excursions at centennial scale or better. We here report a multidecadally resolved Chinese stalagmite paleomagnetic record for the 107- to 91-ka interval with closely spaced U-Th ages. The record provides important insights into ancient geomagnetic field behavior of excursional events that reveal repeated centennial–millennial interhemispheric polarity drifts and saw-tooth inclination oscillations with one abrupt centennial reversal transition.

U-Th Dating and Paleomagnetic Analyses

Stalagmite SX11 was collected in a chamber 800 m from the entrance of Sanxing Cave (107°11′ E, 27°22′ N, 2 km in length, 720-m altitude), Guizhou Province, southwestern China (Fig. 1 A and B), in 2011. The stalagmite is 1 m in length and 8 cm in diameter, and it has a candle-like shape and yellow to dark brown color (Fig. 1C). At the micrometer scale, irregularly shaped detrital particles are observed within laminae (*SI Appendix*, Fig. S2). Subsamples with 5-mm thickness were used for U-Th dating to provide 2σ precision of ±10s of years (*Methods Summary*). The stalagmite, which was deposited from 106.66 to 91.23 ka, contains a hiatus from 100.81 to 98.77 ka (Fig. 1C and *SI Appendix*, Figs. S3 and S4).

One hundred ninety-four subsamples were cut along horizontal growth laminae to avoid possible distorted paleomagnetic directions at stalagmite slope edges (*Methods Summary*). The natural remanent magnetization (NRM) ranges from 10^{-3} to 10^{-5} A/m and averages 10^{-4} A/m. Alternating field (AF) demagnetization results for most (180 of 194) subsamples indicate the presence of a weak viscous remanent magnetization (VRM) that is removed after AF treatment at 10–25 mT. At high demagnetization fields, the NRM is dominated by one stable paleomagnetic component that generally decays linearly to the origin of demagnetization diagrams and that defines the characteristic remanent magnetization (ChRM) with AF < 50 mT (*Methods Summary*, Fig. 2 A and C, *SI Appendix*, Fig. S5, and Dataset S2). Thermal demagnetization of a three-axis isothermal remanent magnetization (IRM) (27) indicates that the soft component (B_{cr} < 50 mT) is fully thermally demagnetized at 575 °C, which indicates that the ChRM carrier is dominantly magnetite (Fig. 2 B and D and *SI Appendix*, Fig. S6). The ratio of anhysteretic remanent magnetization (ARM) to saturation isothermal remanent magnetization applied in a 1-T pulse field
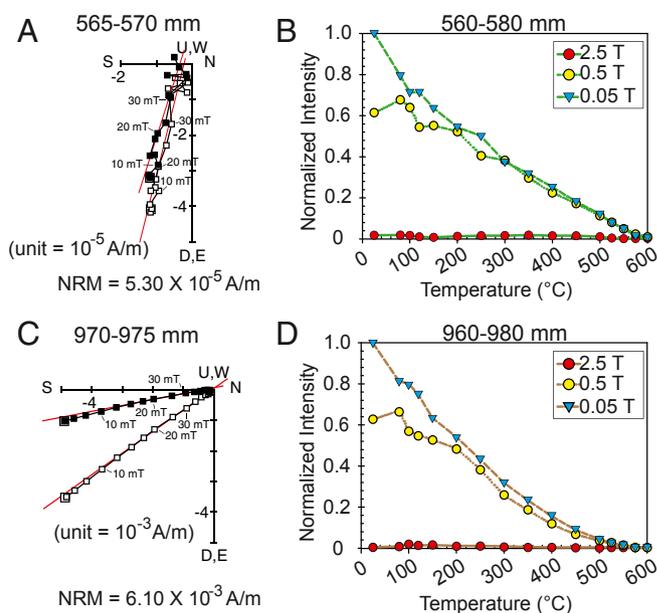
Fig. 2. Orthogonal projections of AF demagnetization results for the NRM and thermal demagnetization results for a three-axis IRM. Typical orthogonal vector component plots for depth intervals of (A) 565–570 and (C) 970–975 mm with vector endpoints projected onto the vertical (white squares) and horizontal (black squares) planes. Letters of E, W, S, N, U, and D denote east, west, south, north, up, and down, respectively. ChRM line fits (red lines) indicate the presence of one stable component with NRM values of 6.10 × 10^{-3} A/m at 970–975 mm and as low as 5.30 × 10^{-5} A/m at 565–570 mm. Thermal demagnetization curves for a three-axis IRM at depth intervals of (B) 560–580 and (D) 960–980 mm imparted with fields of 2.5 (red circles), 0.5 (yellow circles), and 0.05 T (blue triangles). Unblocking up to 575 °C indicates that magnetite is consistently the dominant magnetic mineral.

($SIRM_{1T}$) suggests that the magnetite particles are in the single domain to vortex state size range (*SI Appendix*, Fig. S7). These properties are typical of the pedogenic and detrital magnetite particles that are likely to be delivered to the stalagmite by drip waters. The stability of the recorded paleomagnetic directions throughout the stalagmite (*SI Appendix*, Fig. S5) confirms that the magnetite particles must be in this magnetically stable particle size range. A one-component ChRM with a signal dominated by magnetite indicates that the magnetic particles acquired a depositional remanent magnetization without chemical alteration/precipitation of magnetic carriers during stalagmite growth (28).

Geomagnetic excursions are often defined as a deviation of the virtual geomagnetic pole (VGP) from the normal paleosecular variation range (NPSVR) (29). Stalagmite SX11 was not oriented azimuthally, and VGPs could not be calculated from paleomagnetic directions. NPSVR for inclination at the site was calculated with a paleosecular variation model for VGP scatter (30). The gradient color bands in Fig. 3B indicate inclination distributions from modeled paleosecular variation for normal (yellow in Fig. 3B) and reversed (blue in Fig. 3B) polarities at 27°22′ N, where the most intense color expresses the highest probability; geocentric axial dipole field inclinations for both polarities ±45.8° are also plotted with dashed lines in Fig. 3B (*Methods Summary* and *SI Appendix*, Fig. S8). Two excursions, post-Blake 1 (PB1) and PB2, which are defined based on inclination, are recorded in the stalagmite inclination record at 105.8–103.5 and 98.5–92.0 ka, respectively (Fig. 3). These excursions coincide with the PB excursion (PBE) events at 105 and 95 ka, respectively, which were discovered in Lac du Bouchet, France (31). $^{40}Ar/^{39}Ar$ dating of lava flows from Lipari Island and New Mexico indicates that the beginning of the PBE was at
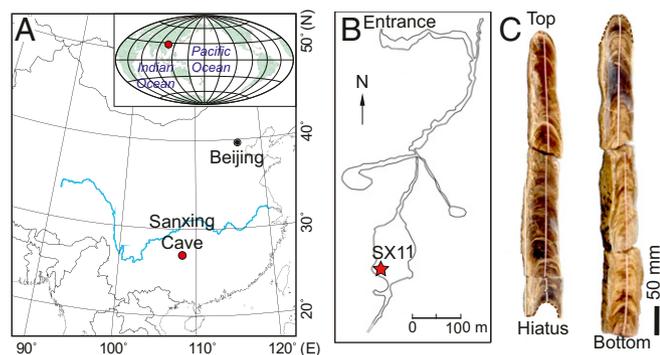

Fig. 1. Sampling location and photograph of Sanxing stalagmite SX11. (A) Location map of Sanxing Cave (red circle). (B) The sampling site of SX11 in the cave chamber (red star). (C) Stalagmite photograph. The white line is a tape measure, and the dashed brown curved line denotes a hiatus at a depth of 45.5 cm.

Fig. 3. Paleomagnetic record for Sanxing stalagmite SX11 at 107–91 ka. (*A*) Two excursions, PB1 and PB2, are indicated in the magnetostratigraphic column. (*B*) Inclination record with 95% confidence limit of ChRM (calculated following ref. 51 and shaded in gray). ^{230}Th ages and 2σ errors are plotted. Numbers with uncertainties are ^{230}Th ages per data point (unit: years before AD 1950). Ages in italics were calculated using the linear age model to interpolate between two adjacent determined ^{230}Th ages with propagated errors. Horizontal dashed lines are inclinations for a geocentric axial dipole field at the site. Yellow and blue color gradient bands denote the probability distributions of modeled paleosecular variation at 27°22′ N for normal and reversed polarity, respectively. The letters *a–f* and numbers *1–4* represent different intervals of geomagnetic field behavior described in the text. (*C*) Relative declination record with 95% confidence limit of ChRM (shaded in gray). (*D*) Virtual axial dipole moment (VADM) records of the SINT-800 (blue line), PISO-1500 (red line), and PADM2M (black line) RPI stacks with 95% confidence limits (39–41). The vertical light gray bar indicates the location of the hiatus.

104–105 ka (Lipari: 105 ± 1 ka; New Mexico: 104 ± 12 ka) (17). The PBE is also recorded in Icelandic lava flows at 94 ± 8 ka (32).

For the PB1 excursion, at least three submillennial to millennial directional drift cycles (Fig. 3, *a* and *b*, 650 y; *c* and *d*, 1,100 y; *e* and *f*, 500 y) with inclinations that change from the NPSVR to shallow excursional angles are identified (Fig. 3). The first cycle (PB1-*a* and PB1-*b*) involves a rapid inclination deviation from 27.3° to 0.8° and a westward declination drift of 60° in 100 y (*a* in Fig. 3*B*; inclination enlarged in *SI Appendix*, Fig. S9) followed by a 150-y northward inclination shift back to NPSVR values and an eastward declination drift of 60°. Directions then remain in the NPSVR for 400 y (*b* in Fig. 3*B*; inclination enlarged in *SI Appendix*, Fig. S9). The second cycle (PB1-*c* and PB1-*d* in Fig. 3*B*; inclination enlarged in *SI Appendix*, Fig. S9) has a similar pattern, where the inclination deviated from 49.7° to −2.9° in 70 y (PB1-*c*), rebounded back to NPSVR values in 70 y, and then remained in the NPSVR for 900 y. The counterpart declination change involved a rapid 120° eastward movement followed by westward drift back to NPSVR values (PB1-*d*). The structure of the third cycle (PB1-*e* and PB1-*f*) differs from that of the first two cycles. The inclination deviated slowly from 27.3° to 8.8° in 350 y (PB1-*e*) and then returned in 150 y (PB1-*f*). The declination changed within a 60° range. The PB1-*e* and PB1-*f* record has large uncertainties with low stalagmite growth rates, which prevent clear visualization of field behavior. After 103 ka, inclinations remained within the NPSVR, and relative declinations were roughly constant for at least two millennia.

The PB2 excursion has two large inclination drift cycles (Fig. 3, *1* and *2*, 2,300 y; *3* and *4*, 3,900 y) from 98 to 92 ka (Fig. 3). The cycle at 98–96 ka involved an abrupt drift to full opposite polarity with inclination changing from 30.0° to −64.6° (one data point at 98.22 ka) and a westward declination shift of 120° from 98,360 ± 39 to 98,216 ± 43 y (*1* in Fig. 3*B*; inclination enlarged in *SI Appendix*, Fig. S9) followed by a 1,400-y period with excursional inclinations from −19.5° to −0.1° and an inclination return to NPSVR over 800 y, with declination drifts of >60° (PB2-*2*). The second cycle at 96–92 ka records a reversal process with a gradual 40° inclination shift with four 250-y fluctuations, each recorded by multiple data points, from 62.3° to −20.9°. During this 1,050-y interval of PB2-*3*, the declination rotated eastward by >60° over the first 950 y and rotated westward by >60° during the final 100 y. Through the 2,950-y PB2-*4* interval, excursional inclinations between −9.0° and 3.5° occurred over a 2,350-y period, with declination drifts of >30°. Directions then returned to NPSVR values slowly, with declination rotating >60° eastward in 300 y. The geomagnetic structure of these multimillennial cycles is similar to that of the first two submillennial cycles in the PB1 excursion (*a–b* and *c–d*), although with different timescales.

Asymmetrical Interhemispheric Polarity Oscillations

The multicycle variations during the PBE illustrated in Fig. 3 are also observed for the BE over the 119- to 112-ka interval in a stalagmite from northern Spain (22) that lacks precise age control. Such a detailed multidecadally resolved drift structure is only precisely dated in the Sanxing stalagmite. The multicentennial to millennial inclination drift cycles (Fig. 3*B*) are characterized by an abrupt southward shift and slow relaxation back to the NPSVR (except PB1-*e* and PB1-*f*), which are expressed as an asymmetrical saw-tooth oscillation. For the PB1 excursion, the three observed inclination events only drift to ~0°, whereas one fully reversed polarity direction is observed in the PB2 excursion. The longest saw-tooth inclination oscillation is 4,000 y for the cycle from PB2-*3* to PB2-*4* (Fig. 3*B*), and the shortest is only 650 y for the period from PB1-*a* to PB1-*b*. Even with large differences in oscillation durations, a similar geomagnetic structure is depicted for the multicentennial to millennial cycles with an abrupt southward shift and slower rebound (Fig. 3*B*). The periodicity and amplitude of directional

deviations of saw-tooth oscillations are amplified in PB2 with respect to PB1. The stalagmite BE record from northern Spain has a low inclination departure a few thousand years before the full reversed polarity event (22). The PBE record from SX11 also has a low inclination PB1 period before PB2. The low inclination event could be a precursor before the large amplitude geomagnetic excursion.

The most noticeable features of our record are the occurrence of two dynamical changes toward negative inclination at PB2. The one-millennium PB2-*3* drift period from 96.0 to 94.9 ka is characterized by four 250-y fluctuations (Fig. 3*B*). Another abrupt movement occurred in 144 ± 58 y during PB2-*1* (Fig. 3*B* and *SI Appendix*, Fig. S9). These polarity transition periods are much shorter than previously estimated millennial-scale reversal durations from volcanic records (33). The most surprising observation is the abrupt centennial polarity shift at PB2-*1*, which possibly occurred within one century. Such an extremely rapid polarity drift has not been shown before. Previous hotly debated rates from lava (34) and lacustrine sedimentary (35) records suggested extreme directional changes of 1° per week (34) or less than a century for the transition between polarity states (35). However, the rapid reversal indicated by lava flows was rescinded in later studies (36), and the lacustrine records (35) have been suggested (37) and then shown to be affected by chemical remagnetization (38).

Mechanisms of Asymmetrical Polarity Drifts

Transitional field morphologies and underlying physical mechanisms have never been established fully due to the lack of detailed geomagnetic excursion records with precise dating. Our Sanxing stalagmite record offers a radioisotopically dated dynamic view of geomagnetic field behavior on multidecadal to millennial timescales associated with reversals or excursions (Fig. 3 and *SI Appendix*, Fig. S9). The saw-tooth inclination oscillations represent asymmetrical interhemispheric polarity drifts at 105.8–103.5 and 98.5–92.0 ka, respectively (Fig. 3). A rapid reversal event within a century at 98 ka (PB2-*1*) (*SI Appendix*, Fig. S9) coincides with a global relative paleointensity (RPI) minimum (39–41) (Fig. 3*D*), which indicates a strong link between the amplitude of the directional deviation and RPI.

A hypothesis for geomagnetic excursions has suggested that rapid field changes (Fig. 3) are associated with an intrinsically oscillating dynamo during periods with low dipole intensity (42), although exact timescales are unknown. Our stalagmite record provides a precisely radioisotopically dated excursion time series, which reveals that directional geomagnetic stability correlated inversely with field intensity (Fig. 3 *B* and *D*) and that the geodynamo was intrinsically less stable when dipole field intensities were low. Model simulations (43) indicate that, under a low-friction scenario with small Ekman number, disturbances can propagate in Earth's liquid outer core. The enhanced outer core convective flow can generate a geomagnetic field with a particular polarity. This gradually increasing field may become unstable and then eventually collapse as depicted by inclination dynamics during PB2-*3* and PB2-*1*. Ongoing convection continues to produce dynamo action and generates magnetic fields that could have the opposite polarity. Inclination variability shown in Fig. 3 suggests that such a nonlinear process probably repeats several times on centennial to millennial timescales in response to chaotic geomagnetic variations. Our results support the argument that the geodynamo was unstable and that it undergoes continuous change to reestablish a full polarity state between occasional collapses (43).

Full geomagnetic polarity reversals are relatively rare (3). The intensity of Earth's magnetic field varies continuously, and it has decreased by ~10% over the past century, which has led to suggestions of an impending reversal (11, 12), although it is controversial (44). Our Sanxing stalagmite record indicates that

short-lived but rapid field changes occur on centennial time-scales when the geomagnetic field intensity decreases into a reversal or excursion. Such rapid geomagnetic changes can disturb animal navigation (45), damage satellites, and disturb radio communications (46). A much-improved view of past geomagnetic fluctuations without the smoothing or temporally aliased spot readings provided by sedimentary or volcanic archives is, thus, important for obtaining additional insights into geomagnetic transition processes.

Methods Summary

Subsampling. The SX11 stalagmite was cut into halves along its growth axis. One-half of the stalagmite was cut into 8-cm^3 cubic subsamples along its central axis for thermal demagnetization of a three-axis IRM. One thin section, 20–30 μm in thickness, was prepared at a depth interval of 53–55 cm along the central stalagmite axis for screening micrometer-scale minerals. Another halved stalagmite was cut into a column with a 4-cm^2 cross-section along its central axis perpendicular to horizontal growth laminae. The column was sliced into 194 blocks, with dimensions of 2 (length) × 2 (width) × 0.5 (thickness) cm, containing 5–10% curved laminae for paleomagnetic analyses. After the analyses, 67 block subsamples with 5-mm thickness were selected for U-Th dating.

U-Th Dating and Age Model. U-Th chemistry was conducted in a class-10,000 metal-free clean room with class-100 benches at the High-Precision Mass Spectrometry and Environment Change Laboratory, Department of Geosciences, National Taiwan University (47). Determinations of all isotopic compositions and concentrations were made on a Thermo-Finnigan NEPTUNE multicollector inductively coupled plasma mass spectrometer with Faraday-cup protocols (26). U-Th uncertainties were calculated at the 2σ level and include corrections for procedure blanks, abundance sensitivity, mass discrimination, and the occurrence of isotopes of interest in spike solution. Half-lives of U-Th nuclides used are given in ref. 26. Details of ^{230}Th age calculation are described in ref. 48. U-Th isotopic compositions and ^{230}Th dates are given in Dataset S1. Agreement of duplicated ^{230}Th ages between coeval subsamples at 10 depths (SI Appendix, Fig. S3) indicates the fidelity of our dating approach. The chronology was built by linear interpolation between ^{230}Th ages (before AD 1950). Ages shown in the figures are the determined ^{230}Th ages with 2σ level (Dataset S1) or were calculated using the linear age model and two adjacent determined ages with propagated errors.

Synchrotron X-Ray Microscope, Rock Magnetism, and Paleomagnetism. On the prepared thin section, micrometer-scale minerals within calcium carbonate matrix were inspected at high resolution (up to 30 nm) with synchrotron transmission X-ray microscopic techniques (49) using beamlines BL01A1 and BL01B1 at the Taiwan Light Source, National Synchrotron Radiation Research Center (Hsinchu, Taiwan, Republic of China). For thermal demagnetization of a three-axis IRM (27), fields of 2.5, 0.5, and 0.05 T were applied along three orthogonal sample axes on an MC-1 Pulse Magnetizer to identify

magnetic minerals using coercivity and unblocking temperatures (Fig. 2 *B* and *D* and SI Appendix, Fig. S6).

The stalagmite was not oriented azimuthally; relative declinations were measured with respect to the orientation of the cut half surface. NRM data for the cut block subsamples were obtained using automated stepwise AF demagnetization with a high-resolution cryogenic magnetometer with automatic sample changer (background 2 × 10^{-7} A/m^2) in a magnetically shielded paleomagnetic laboratory at the Institute of Geology and Geophysics, Chinese Academy of Sciences (Beijing, People's Republic of China). Subsamples were demagnetized with AFs of 2.5, 5.0, 7.5, 10.0, 12.5, 15.0, 17.5, 20, 25, 30, 35, 40, 45, 50, 55, and 60 mT; test subsamples were also treated at additional steps of 70, 80, 90, and 100 mT. Orthogonal vector component plots were used to determine the ChRM for each subsample. A VRM was removed between 10 and 25 mT for most samples. The principal component analysis method of refs. 50 and 51 was used to estimate ChRM directions with 95% confidence limits for each sample. Demagnetization plots for 180 subsamples decay linearly and generally (155 of 180) to the origin. Unanchored fits were used following ref. 50. Fourteen subsamples with erratic demagnetization behavior were excluded. An ARM was applied with a 100-μT direct current bias field and a 100 mT AF. An SIRM$_{1T}$ was imparted in a 1-T field with an MMPM-10 impulse magnetizer. ARM and SIRM$_{1T}$ were only measured for the uppermost 80 subsamples from stalagmite SX11.

The NPSVR for the sampling site was calculated using the TK03 model (30) and the software of ref. 52. A histogram of inclinations from 20,000 simulations in TK03 (SI Appendix, Fig. S8) at the sample site (latitude 27°22′ N) indicates inclination distributions from modeled paleosecular variation for normal (yellow in SI Appendix, Fig. S8) and reversed (blue in SI Appendix, Fig. S8) polarities (where intense colors indicate high probability and white indicates zero probability). Possible VGP paths during the PBE were calculated by rotating relative declination values counterclockwise by 150° to give a mean value of 0° for the nontransitional interval at 103–101 ka (SI Appendix, Fig. S10).

1. Buffett BA (2000) Earth's core and the geodynamo. *Science* 288:2007–2012.
2. Tarduno JA, et al. (2010) Geodynamo, solar wind, and magnetopause 3.4 to 3.45 billion years ago. *Science* 327:1238–1240.
3. Lowrie W, Kent DV (2013) Geomagnetic polarity timescales and reversal frequency regimes. *Timescales of the Paleomagnetic Field*, eds Channell J, Kent D, Lowrie W, Meert J (American Geophysical Union, Washington, DC), pp 117–129.
4. McElhinny MW, McFadden PL (1999) *Paleomagnetism: Continents and Oceans* (Academic, New York).
5. Channell JET, Hodell DA, Singer BS, Xuan C (2010) Reconciling astrochronological and ^{40}Ar/^{39}Ar ages for the Matuyama-Brunhes boundary and late Matuyama Chron. *Geochem Geophys Geosyst* 11:Q0AA12.
6. Singer BS (2014) A Quaternary geomagnetic instability time scale. *Quat Geochronol* 21:29–52.
7. Laj C, Channell JET (2015) Geomagnetic excursions. *Treatise on Geophysics*, ed Schubert G (Elsevier, Amsterdam), 2nd Ed, Vol 5, pp 343–383.
8. Roberts AP (2008) Geomagnetic excursions: Knowns and unknowns. *Geophys Res Lett* 35:L17307.
9. Kitaba I, Hyodo M, Katoh S, Dettman DL, Sato H (2013) Midlatitude cooling caused by geomagnetic field minimum during polarity reversal. *Proc Natl Acad Sci USA* 110: 1215–1220.
10. Maffei ME (2014) Magnetic field effects on plant growth, development, and evolution. *Front Plant Sci* 5:445.
11. Constable C, Korte M (2006) Is Earth's magnetic field reversing? *Earth Planet Sci Lett* 246:1–16.
12. Laj C, Kissel C (2015) An impending geomagnetic transition? Hints from the past. *Front Earth Sci* 3:61.
13. Matuyama M (1929) On the direction of magnetisation of basalt in Japan, Tyosen and Manchuria. *Proc Imp Acad Jpn* 5:203–205.
14. Opdyke ND, Channell JET (1996) *Magnetic Stratigraphy* (Academic, New York).
15. Clement BM (2004) Dependence of the duration of geomagnetic polarity reversals on site latitude. *Nature* 428:637–640.
16. Cande SC, Kent DV (1995) Revised calibration of the geomagnetic polarity timescale for the Late Cretaceous and Cenozoic. *J Geophys Res* 100:6093–6095.
17. Singer BS, Guillou H, Jicha BR, Zanella E, Camps P (2014) Refining the Quaternary Geomagnetic Instability Time Scale (GITS): Lava flow recordings of the Blake and Post-Blake excursions. *Quat Geochronol* 21:16–28.
18. van Zijl JSV, Graham KWT, Hales AL (1962) The palaeomagnetism of the Stormberg Lavas. II. The behaviour of the magnetic field during a reversal. *Geophys J R Astron Soc* 7:169–182.
19. Channell JET, Lehman B (1997) The last two geomagnetic polarity reversals recorded in high-deposition-rate sediment drifts. *Nature* 389:712–715.
20. Valet J-P, Meynadier L, Simon Q, Thouveny N (2016) When and why sediments fail to record the geomagnetic field during polarity reversals. *Earth Planet Sci Lett* 453:96–107.
21. Latham AG, Schwarcz HP, Ford DC, Pearce GW (1979) Palaeomagnetism of stalagmite deposits. *Nature* 280:383–385.
22. Osete M-L, et al. (2012) The Blake geomagnetic excursion recorded in a radiometrically dated speleothem. *Earth Planet Sci Lett* 353–354:173–181.
23. Lascu I, Feinberg JM, Dorale JA, Cheng H, Edwards RL (2016) Age of the Laschamp excursion determined by U-Th dating of a speleothem geomagnetic record from North America. *Geology* 44:139–142.
24. Kirschvink JL, Kopp RE, Raub TD, Baumgartner CT, Holt JH (2008) Rapid, precise, and high-sensitivity acquisition of paleomagnetic and rock-magnetic data: Development of a low-noise automatic sample changing system for superconducting rock magnetometers. *Geochem Geophys Geosyst* 11:Q05Y01.

25. Shen C-C, et al. (2012) High-precision and high-resolution carbonate ^{230}Th dating by MC-ICP-MS with SEM protocols. *Geochim Cosmochim Acta* 99:71–86.
26. Cheng H, et al. (2013) Improvements in ^{230}Th dating, ^{230}Th and ^{234}U half-life values, and U–Th isotopic measurements by multi-collector inductively coupled plasma mass spectrometry. *Earth Planet Sci Lett* 371–372:82–91.
27. Lowrie W (1990) Identification of ferromagnetic minerals in a rock by coercivity and unblocking temperature properties. *Geophys Res Lett* 17:159–162.
28. Strauss BE, et al. (2013) The origin of magnetic remanence in stalagmites: Observations from electron microscopy and rock magnetism. *Geochem Geophys Geosyst* 14:5006–5025.
29. Vandamme D (1994) A new method to determine paleosecular variation. *Phys Earth Planet Inter* 85:131–142.
30. Tauxe L, Kent DV (2004) A simplified statistical model for the geomagnetic field and the detection of shallow bias in paleomagnetic tnclinations: Was the ancient magnetic field dDipolar? *Timescales of the Paleomagnetic Field*, eds Channell J, Kent D, Lowrie W, Meert J (American Geophysical Union, Washington, DC), pp 101–115.
31. Thouveny N, Creer KM, Blunk I (1990) Extension of the Lac du Bouchet palaeomagnetic record over the last 120,000 years. *Earth Planet Sci Lett* 97:140–161.
32. Jicha BR, et al. (2011) New age for the Skálamælifell excursion and identification of a global geomagnetic event in the late Brunhes chron. *Earth Planet Sci Lett* 310:509–517.
33. Valet J-P, Fournier A, Courtillot V, Herrero-Bervera E (2012) Dynamical similarity of geomagnetic field reversals. *Nature* 490:89–93.
34. Coe RS, Prevot M, Camps P (1995) New evidence for extraordinarily rapid change of the geomagnetic field during a reversal. *Nature* 374:687–692.
35. Sagnotti L, et al. (2014) Extremely rapid directional change during Matuyama-Brunhes geomagnetic polarity reversal. *Geophys J Int* 199:1110–1124.
36. Coe RS, Jarboe NA, Le Goff M, Petersen N (2014) Demise of the rapid-field-change hypothesis at Steens mountain: The crucial role of continuous thermal demagnetization. *Earth Planet Sci Lett* 400:302–312.
37. Valet J-P, Fournier A (2016) Deciphering records of geomagnetic reversals. *Rev Geophys* 54:410–446.
38. Evans ME, Muxworthy AR (2018) A re-appraisal of the proposed rapid Matuyama–Brunhes geomagnetic reversal in the Sulmona Basin, Italy. *Geophys J Int* 213:1744–1750.
39. Guyodo Y, Valet J-P (1999) Global changes in intensity of the Earth's magnetic field during the past 800 kyr. *Nature* 399:249–252.
40. Channell JET, Xuan C, Hodell DA (2009) Stacking paleointensity and oxygen isotope data for the last 1.5 Myr (PISO-1500). *Earth Planet Sci Lett* 283:14–23.
41. Ziegler LB, Constable CG, Johnson CL, Tauxe L (2011) PADM2M: A penalized maximum likelihood model of the 0–2 Ma palaeomagnetic axial dipole moment. *Geophys J Int* 184:1069–1089.
42. Busse FH, Simitev RD (2008) Toroidal flux oscillation as possible cause of geomagnetic excursions and reversals. *Phys Earth Planet Inter* 168:237–243.
43. Zhang K, Gubbins D (2000) Is the geodynamo process intrinsically unstable? *Geophys J Int* 140:F1–F4.
44. Brown M, Korte M, Holme R, Wardinski I, Gunnarson S (2018) Earth's magnetic field is probably not reversing. *Proc Natl Acad Sci USA* 115:5111–5116.
45. Tian L-X, Pan Y-X, Metzner W, Zhang J-S, Zhang B-F (2015) Bats respond to very weak magnetic fields. *PLoS One* 10:e0123205.
46. Stevenson DJ (2003) Planetary magnetic fields. *Earth Planet Sci Lett* 208:1–11.
47. Shen C-C, et al. (2003) Measurement of attogram quantities of ^{231}Pa in dissolved and particulate fractions of seawater by isotope dilution thermal ionization mass spectroscopy. *Anal Chem* 75:1075–1079.
48. Shen C-C, et al. (2008) Variation of initial ^{230}Th/^{232}Th and limits of high precision U–Th dating of shallow-water corals. *Geochim Cosmochim Acta* 72:4201–4223.
49. Wang C-C, et al. (2015) Evolution and function of dinosaur teeth at ultramicrostructural level revealed using synchrotron transmission X-ray microscopy. *Sci Rep* 5:15202.
50. Heslop D, Roberts AP (2016) Analyzing paleomagnetic data: To anchor or not to anchor? *J Geophys Res* 121:7742–7753.
51. Heslop D, Roberts AP (2016) Estimation and propagation of uncertainties associated with paleomagnetic directions. *J Geophys Res* 121:2274–2289.
52. Tauxe L, et al. (2016) PmagPy: Software package for paleomagnetic data analysis and a bridge to the Magnetics Information Consortium (MagIC) Database. *Geochem Geophys Geosyst* 17:2450–2463.

Chou et al.